frontiers | Frontiers in Energy Research

TYPE Original Research
PUBLISHED 03 July 2024
DOI 10.3389/fenrg.2024.1417360

OPEN ACCESS

EDITED BY
Joshuva Arockia Dhanraj,
Dayananda Sagar University, India

REVIEWED BY
Ioan Viorel Banu,
University of Bacău, Romania
Kenneth E. Okedu,
Melbourne Institute of Technology, Australia
Roberto Quintal Palomo,
Universidad Autónoma de Yucatán, Mexico
Youcef Belkhier,
École Navale, France

*CORRESPONDENCE
Lin Cheng,
419033106@qq.com

RECEIVED 14 April 2024
ACCEPTED 04 June 2024
PUBLISHED 03 July 2024

CITATION
Cheng L, Wang J, Ke X, Han Z and Ai D (2024), Voltage stability analysis considering dynamic interaction for power systems integrated with multi-PMSGs.
Front. Energy Res. 12:1417360.
doi: 10.3389/fenrg.2024.1417360

Voltage stability analysis considering dynamic interaction for power systems integrated with multi-PMSGs

Lin Cheng[1]*, Jili Wang[2], Xianbo Ke[2], Zhiyong Han[3] and Dongping Ai[3]

[1]School of Electrical Engineering, Xi'an Jiaotong University, Xi'an, China, [2]Northwest Branch of State Grid Corporation of China, Xi'an, China, [3]China Electric Power Research Institution, Beijing, China

This paper presents the dynamic voltage stability index based on the voltage oscillation loop for power systems integrated with multiple permanent magnet synchronous generators (PMSGs) to assess the dynamic interaction on voltage stability. First, the model of power systems integrated with multi-PMSGs using a Q−V sensitivity matrix as feedback to connect all PMSGs is established. The transfer function model between voltage and reactive power is derived, and the voltage oscillation loop can be derived, which exists in each PMSG. Next, the dynamic voltage stability index is theoretically derived and given, the impact of dynamic interaction among multi-PMSGs on voltage stability can be quantified, and the source of voltage oscillation can be identified and determined. Then, the voltage stability is recovered by shedding the trouble-making PMSG. The parameters of PMSGs could be tuned with the guidance of the dynamic voltage stability index to reduce the risk of voltage oscillation. Finally, the example of a test system with PMSGs is used to validate the correctness of the dynamic stability index.

KEYWORDS

dynamic interaction, permanent magnet synchronous generators, voltage stability index, voltage oscillation loop, power systems

1 Introduction

Wind power has been applied extensively in many nations as a rich and clean renewable energy source (Kroposki et al., 2017; Wang X. et al., 2015). Among all kinds of wind turbine generators (WTGs), permanent magnet synchronous generators (PMSGs) can be widely used because of its high efficiency and reliability (Li et al., 2012; Sanchez et al., 2012). However, the risk of power angle instability, voltage instability, and frequency instability might increase when power electronic converters are used to link massive amounts of wind generators to the power system. At home and abroad, accidents caused by grid-connected WTGs have been reported recently (Wang L. et al., 2015; Adams et al., 2012), such as the wind farm located in Hebei Province of North China (Wang L. et al., 2015), the Harmi area of West China (Liu et al., 2017), and Texas of the USA (Adams et al., 2012), subsequently causing the tripping of a great number of WTGs and damage to crowbar circuits. These accidents have brought serious challenges to power angle stability, voltage stability, and frequency stability (Rakhshani et al., 2019), which are coupled with each other during the disturbances. In order to improve the stability of renewable energy grid-connected systems,

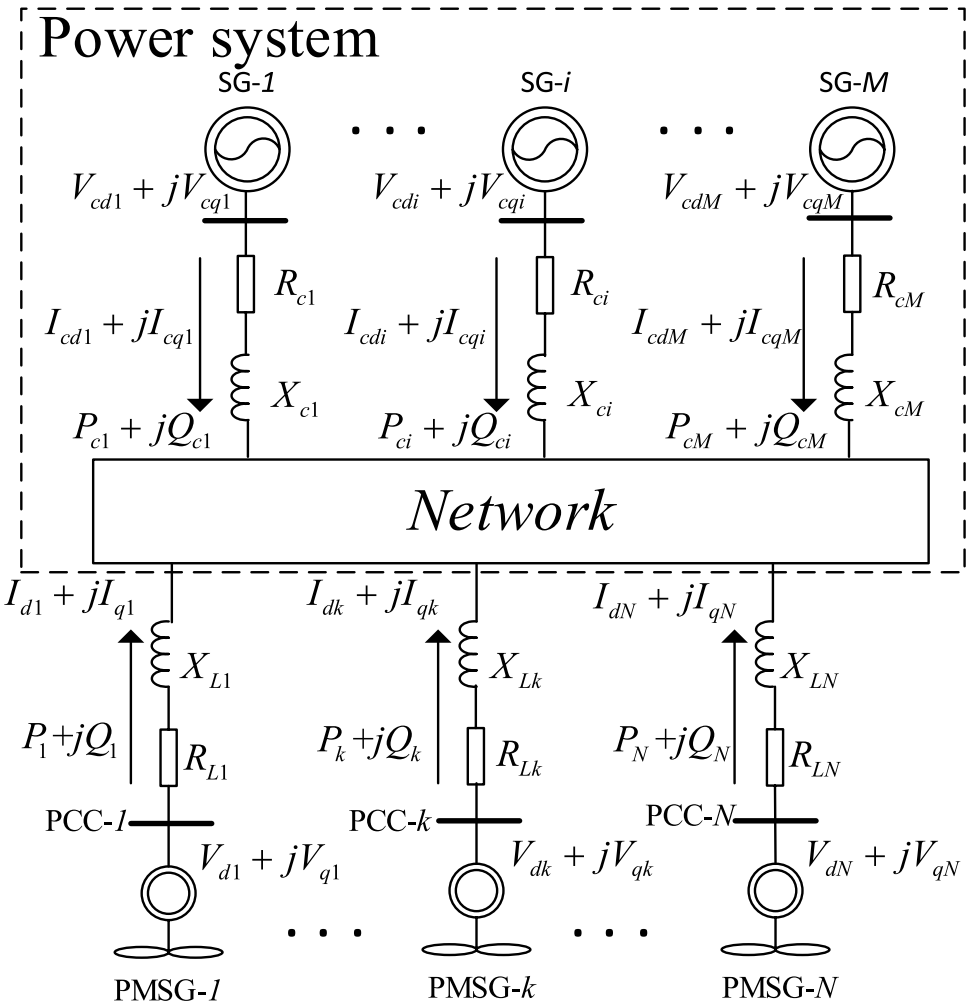

FIGURE 1
Power system with multi-PMSGs.

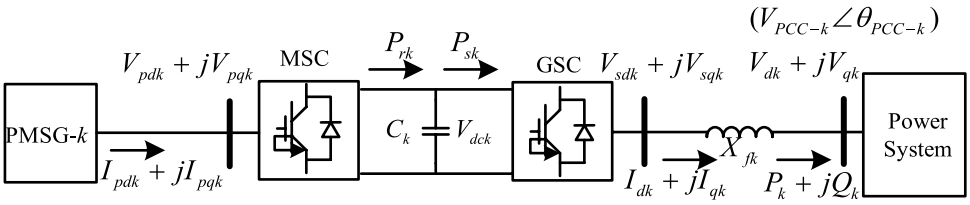

FIGURE 2
PMSG-*k* connected to the power system.

scholars have conducted extensive research. Belkhier and Oubelaid (2024) provided a solution to address the intermittent and stochastic nature of renewable energy management and improve the efficiency of energy systems. A novel control approach is proposed by Khosravi et al. (2023) to improve the stability of hybrid AC/DC microgrids. Dashtdar et al. (2022) provided a new protection method for DC microgrids based on the Fourier transform. Wijnhoven et al. (2014) discussed a selection of control aspects that are important for the negative sequence current injection of type 4 wind turbines. A new WT and VSC-HVDC control method is proposed by Erlich (2017), which can determine the reference voltage directly.

Meanwhile, voltage stability is gaining more attention due to the high penetration of wind generation, and scholars have studied some strategies to improve voltage stability (Ou et al., 2016; Liu and Sun, 2014). Ou et al. (2016); Sravan Kumar et al. (2014) improved voltage stability through the coordination of reactive power. The method of coordinated dynamic VAR source placement is applied for voltage

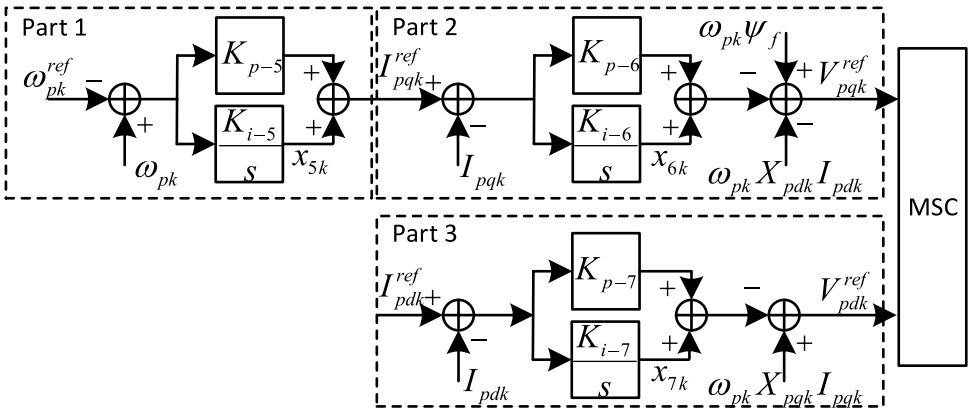

FIGURE 3
MSC vector control of PMSG-*k*.

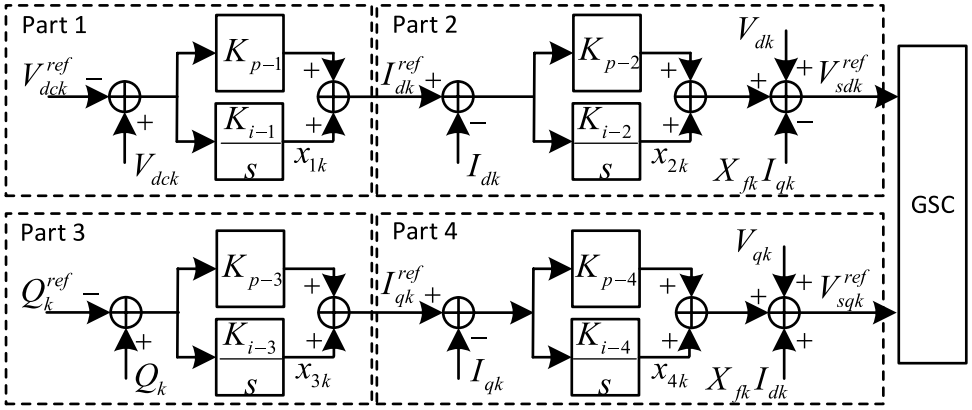

FIGURE 4
GSC vector control of PMSG-*k*.

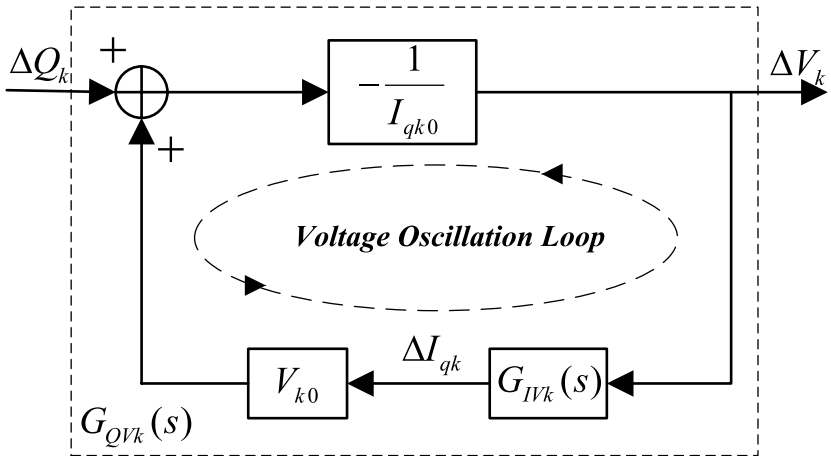

FIGURE 5
Configuration of the voltage oscillation loop of PMSG-*k*.

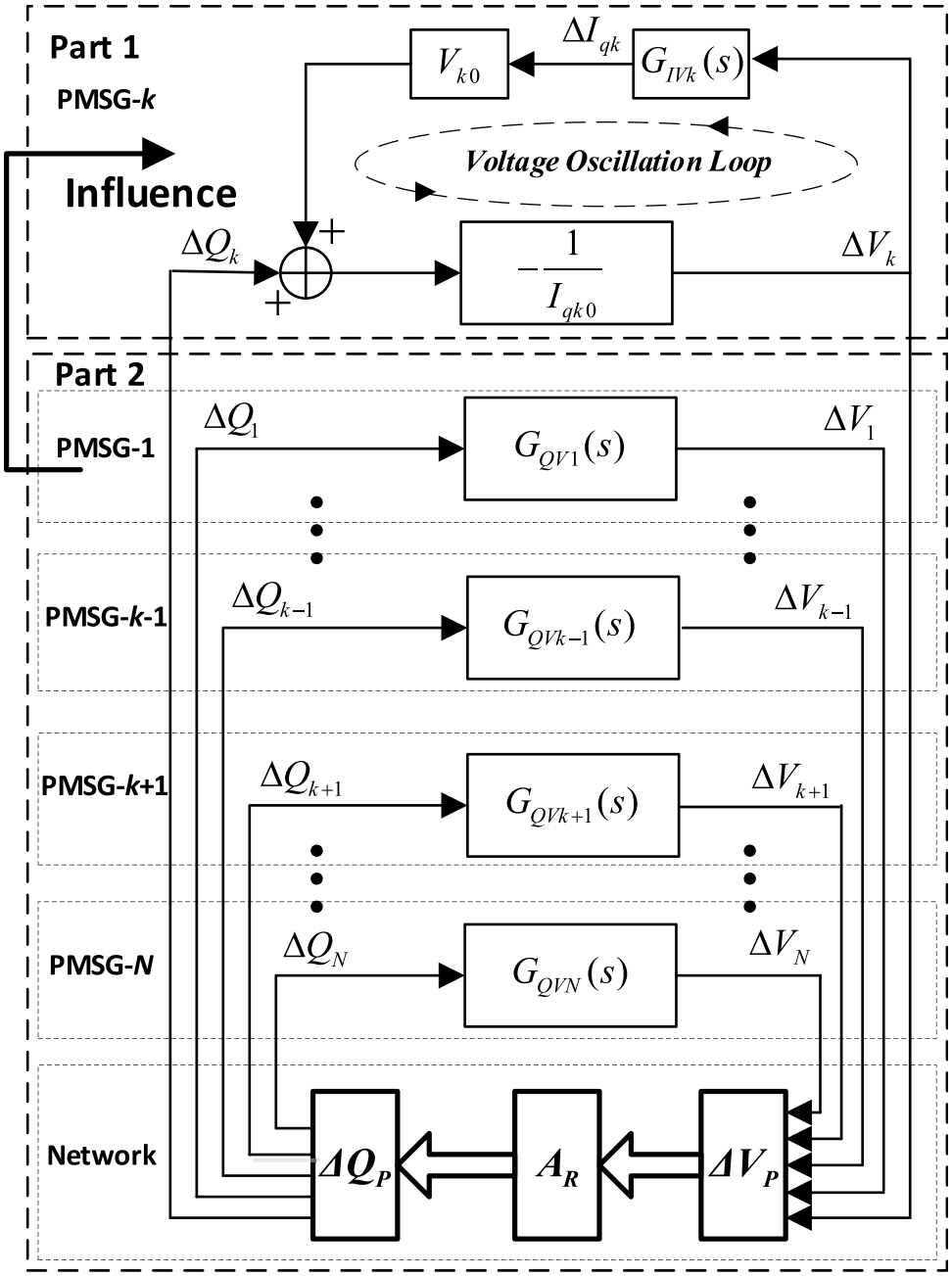

FIGURE 6
Interconnected linearized model of the system with PMSGs.

stability enhancement by Liu et al. (2018); Chi and Xu (2020). The voltage stability and control of offshore wind farms with AC collection and HVDC transmission are investigated through impedance models by Liu and Sun (2014). Voltage stability is more complex with the dynamic interaction among the dynamic units, such as synchronous and wind generators (Qian et al., 2016). Hence, proposing the voltage stability index to evaluate dynamic interaction quantitatively is necessary.

Numerous researchers have developed techniques for assessing the voltage stability of power systems with wind generators, including the continuous power flow method, probability analysis method, and bifurcation theory method. Vittal et al. (2010) provided a detailed methodology to assess the influence of wind turbine generators on the static voltage stability of the power system by combining economic dispatch, power flow, unit dedication, and past time-series information. Rawat and Vadhera (2020) proposed a method to analyze the stable state probabilistic voltage stability margins considering generation and load demand uncertainty. The model is presented to analyze the static voltage stability of the system integrated with WTGs based on bifurcation theory by Tourandaz Kenari et al. (2019), and the probabilistic index can be used to examine the probability risk of voltage collapse.

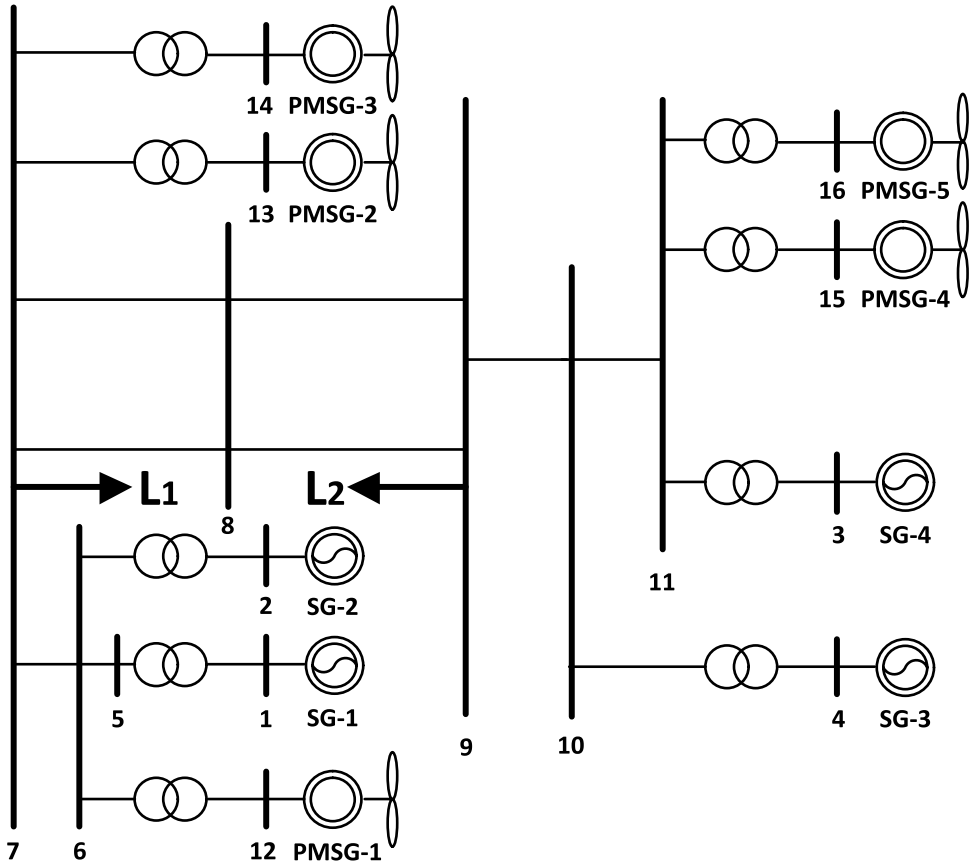

FIGURE 7
Four-machine two-area system integrated with PMSGs.

TABLE 1 Computational results of the dynamic index from each of the rest of PMSGs—study case 1.

Source of the influence	Amount of the index	Source of the influence	Amount of the index
PMSG-2	2.0210	PMSG-4	0.0032
PMSG-3	26.8907	PMSG-5	−0.1001

However, the methods proposed above focus on steady voltage stability. With the dynamic time scale of the power system becoming shorter due to the significant penetration of wind power, the dynamic characteristics of voltage stability cannot be neglected. The scholars have conducted meaningful research studies on the dynamic voltage stability of the power system integrated with WTGs. Venkatesh et al. (2007) presented a dynamic voltage collapse index programmed into a microprocessor-based relay to reflect the risk of voltage collapse over the feeder connecting WTGs. Baa Wafaa and Dessaint (2018) proposed an improved voltage stability index to assess the stability of the system with WTG integration by considering optimal power flow. Su et al. (2019) focused on the dynamic interaction between WTGs and induction motor loads and examined the dynamic voltage stability process from the modal coupling aspect.

As the quantity of WTG grows, the influence of dynamic interactions between multiple wind turbine generators on voltage stability is becoming more dominant. However, the dynamic interactions that exist in multiple wind turbine generators are rarely considered in terms of voltage stability, especially when quantifying the influence of each remaining wind generator on the voltage stability of a selected wind generator in a system with multiple wind turbine generators. Therefore, the paper presents the dynamic voltage stability index for a system integrated with multi-PMSGs based on the voltage oscillation loop, and the index proposed can quantify the influence of dynamic interaction among multi-PMSGs on voltage stability.

The proposed method is more suitable for the analysis of dynamic voltage stability than the continuous power flow method (Vittal et al., 2010), probability analysis method (Rawat and Vadhera, 2020), and bifurcation theory method (Tourandaz Kenari et al., 2019), rather than being limited to analyzing steady voltage stability. Compared with the methods proposed by Venkatesh et al. (2007); Baa Wafaa and Dessaint (2018), this

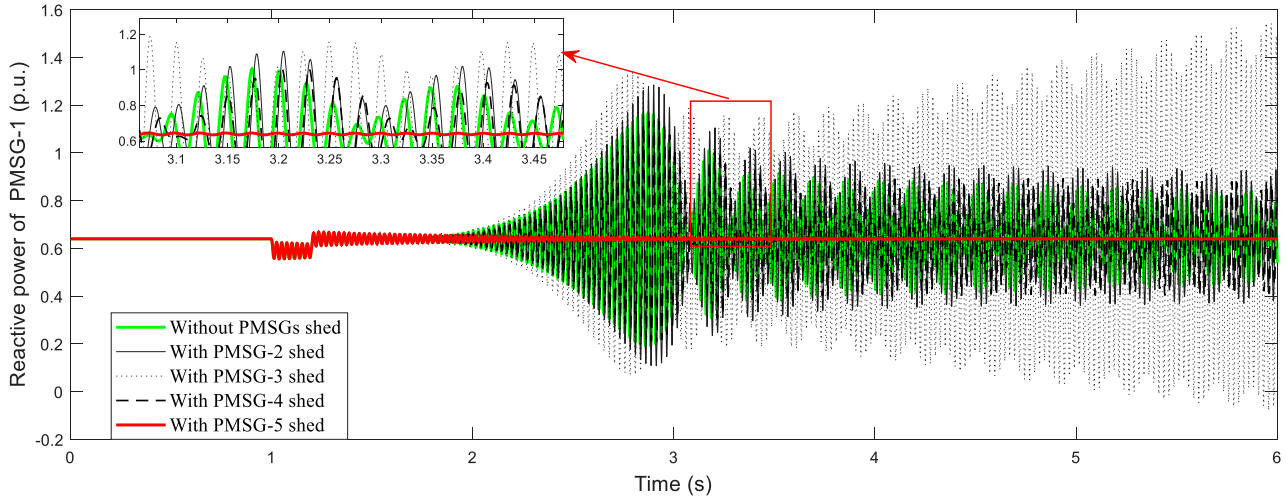

FIGURE 8
Dynamic responses of reactive power of PMSG-1 with different PMSG shed.

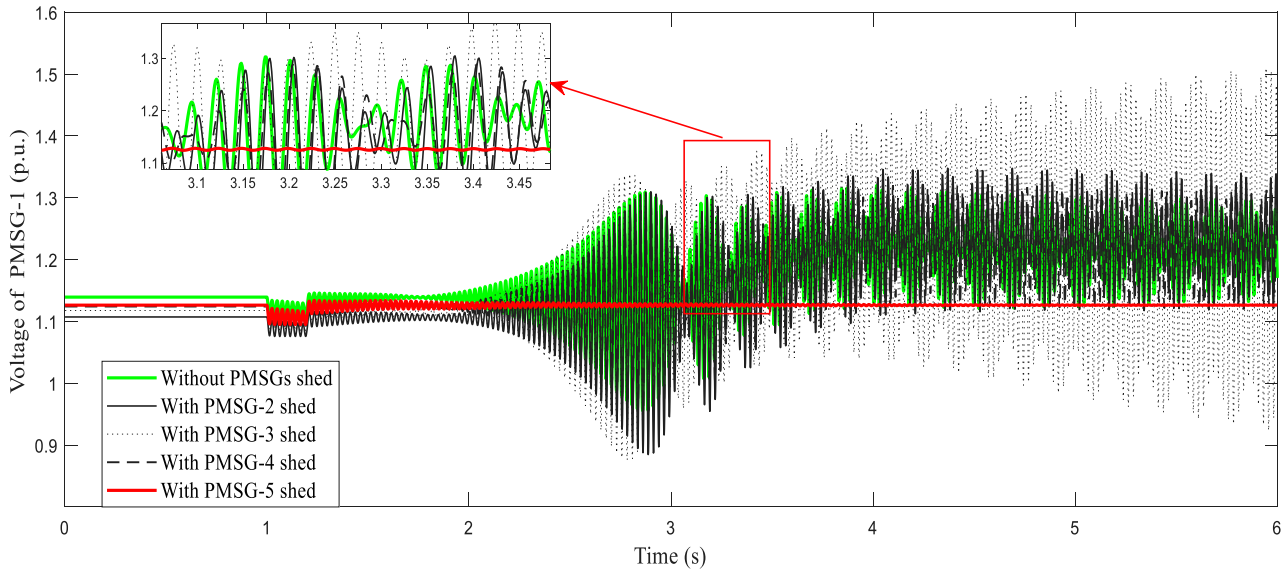

FIGURE 9
Dynamic responses of voltage of PMSG-1 with different PMSG shed.

method can be used to analyze the impact of dynamic interaction on dynamic voltage stability. Su et al. (2019) analyzed the dynamic interaction between WTGs and induction motor loads but did not quantitatively analyze the dynamic interaction among each WTG. Harmonic modeling of the wind turbine induction generator is presented by García et al. (2018), and the method analyzes the harmonic interaction between the wind power generator and the power system, but it is difficult to analyze the dynamic interaction among wind power generators considering the voltage characteristics. Therefore, the proposed method has improved the shortcomings of the methods proposed by Su et al. (2019); García et al. (2018).

In Section 2, the interconnected model of the power system integrated with multi-PMSGs is proposed, and the voltage oscillation loops that exist between PMSGs are derived. In Section 3, the dynamic voltage stability index based on the voltage oscillation loop is introduced, and the theoretical derivation and calculation steps of the index are presented. Based on the voltage stability index, the source of voltage oscillation can be identified and the parameter tuning of PMSGs can be guided. In Section 4, the validity of the proposed dynamic voltage stability index is tested under different scenarios in the test system. Section 5 summarizes the novelty and main contributions. The novelty and

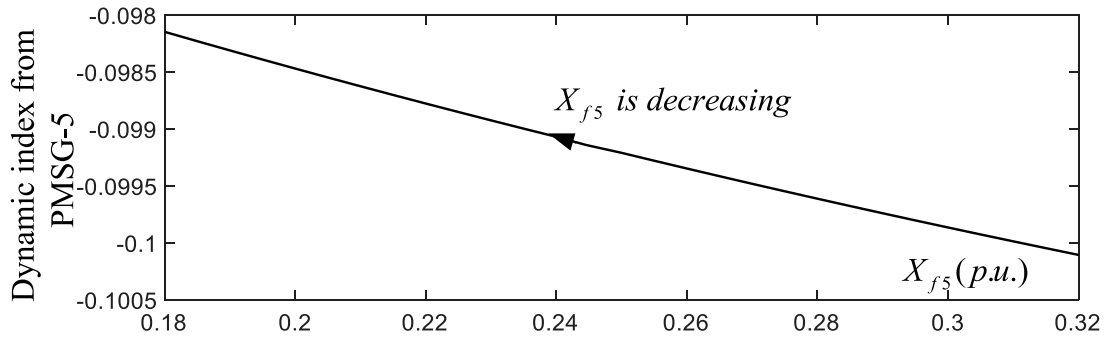

FIGURE 10
Variation curve of the dynamic index of PMSG-5.

TABLE 2 Computational results of the dynamic index from each of the rest of PMSGs—study case 2.

Source of the influence	Amount of the index	Source of the influence	Amount of the index
PMSG-2	2.0210	PMSG-4	0.0032
PMSG-3	26.8914	PMSG-5	−0.0981

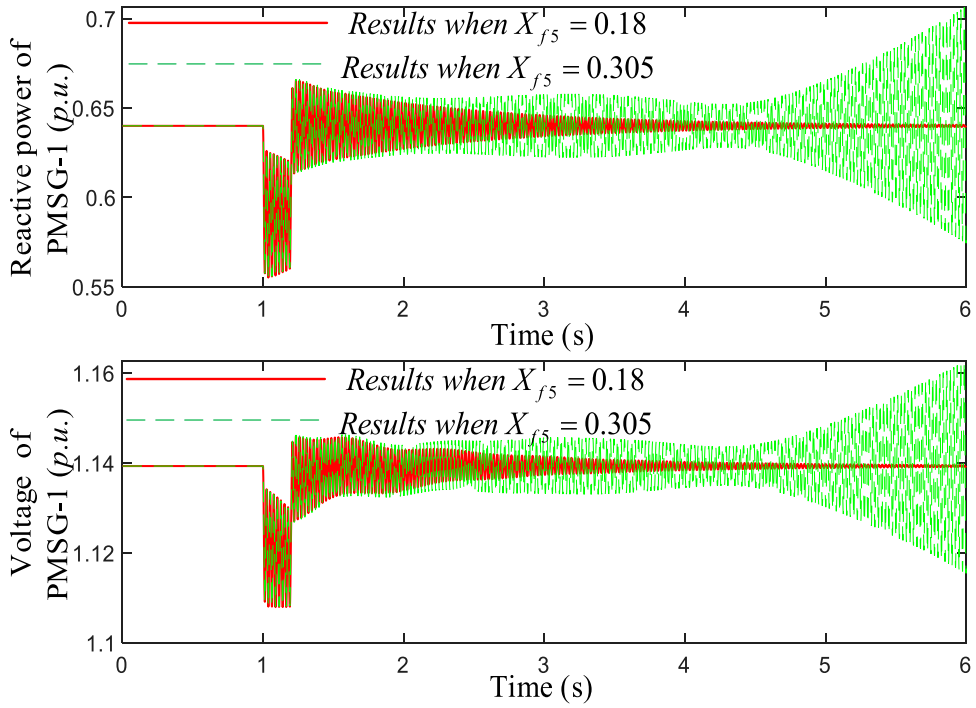

FIGURE 11
Dynamic responses of reactive power and voltage of PMSG-1 under different conditions of the filtering reactor.

contributions of the paper are mainly reflected in four aspects: 1) the transfer function model between voltage and reactive power at the point of common coupling is derived by combining the dynamic equation of PMSGs and the power equation at the point of common coupling; then the voltage oscillation loop of PMSG is derived. 2) The dynamic model of power systems integrated with multi-PMSGs using the Q–V sensitivity matrix as feedback to connect all PMSGs is established. 3) The dynamic voltage stability index is theoretically derived and given, the impact of dynamic interaction among multi-PMSGs on voltage stability can be

TABLE 3 Computational results of the dynamic index from each of the rest of PMSGs—study case 2.

Source of the influence	Amount of the index		Source of the influence	Amount of the index	
	X_{f5} = 0.305	X_{f5} = 0.18		X_{f5} = 0.305	X_{f5} = 0.18
PMSG-2	0.2125	0.2125	PMSG-4	0.0004	0.0004
PMSG-3	2.1256	2.1259	PMSG-5	−0.0104	−0.0096

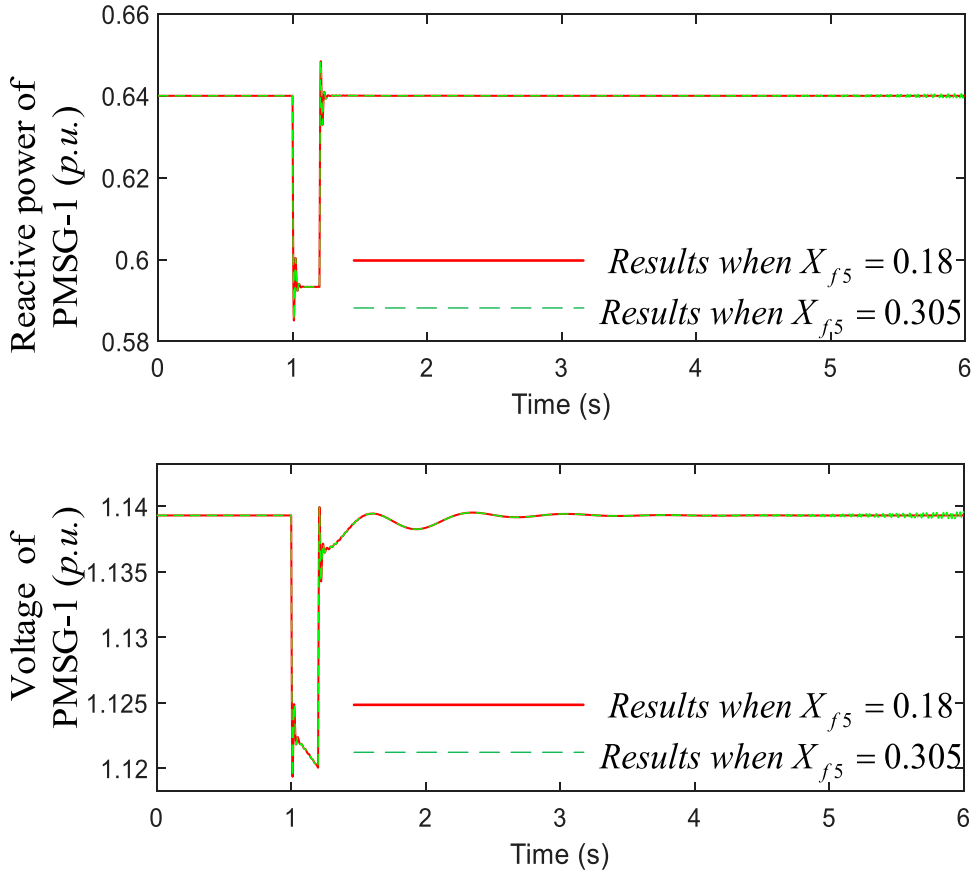

FIGURE 12
Dynamic responses of reactive power and voltage of PMSG-1 under different conditions of the filtering reactor.

quantified, the source of voltage oscillation can be identified and determined, and then the voltage stability is recovered by shedding the trouble-making PMSG. 4) The parameters of PMSGs could be tuned with the guidance of the dynamic voltage stability index to reduce the risk of voltage oscillation.

2 Model of power systems with multi-PMSGs

The configuration of the power system integrated with multi-PMSGs is shown in Figure 1, and PMSGs are connected to N nodes. X_{Lk} and R_{Lk} are the inductance and resistance of the kth line, which connects the PMSG and power system. V_k is the voltage of PMSG-k, and $P_k + jQ_k$ and $I_{dk} + jI_{qk}$ indicate the power and current output of kth PMSG, respectively.

An interconnected model of the transfer function of the whole system is established to analyze the voltage stability of power system integrated with multi-PMSGs.

2.1 Dynamic model of the power system

Figure 1 depicts the precise structure of the power system. There are M SGs and N points of common coupling (PCC) of PMSGs. Denote $I_{cdi} + jI_{cqi}$ and $P_{ci} + jQ_{ci}$ as the power and the current output of ith SG. X_{ci} and R_{ci} are the inductance and resistance of the

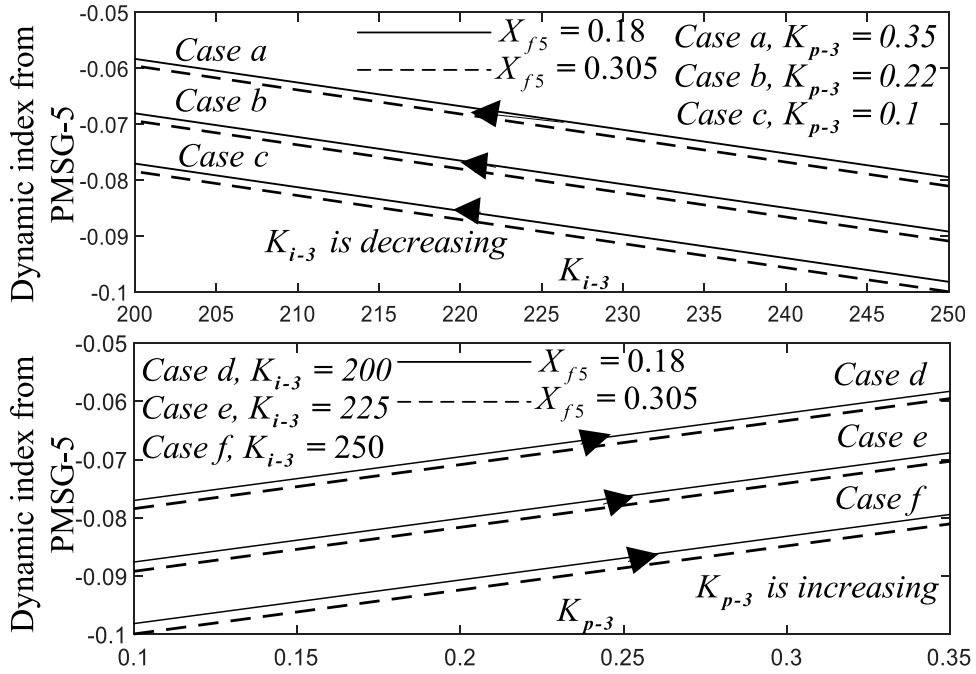

FIGURE 13
Variation curves of the dynamic index of PMSG-5 when the parameters are changing.

*i*th line, and V_{ci} is the voltage of SG-*i*. The state-space model of SG-*i* can be established as follows (Du et al., 2016):

$$\begin{aligned} \frac{d}{dt}\boldsymbol{\Delta X_{ci}} &= \boldsymbol{A_i \Delta X_{ci}} + \boldsymbol{b_{pi}}\Delta P_{ci} + \boldsymbol{b_{qi}}\Delta Q_{ci} \\ \Delta V_{ci} &= \boldsymbol{c_i^T \Delta X_{ci}} + d_{pi}\Delta P_{ci} + d_{qi}\Delta Q_{ci} \end{aligned}, \tag{1}$$

where Δ denotes the deviation of variables and $\Delta \boldsymbol{X_{ci}}$, ($i$=1, 2 . . . , M) represents the SG-*i* variable matrix.

From Eq. 1, the model of SG-*i* can be obtained as

$$\Delta V_{ci} = G_{pi}(s)\Delta P_{ci} + G_{qi}(s)\Delta Q_{ci}, \tag{2}$$

where $\begin{aligned} G_{pi}(s) &= \boldsymbol{c_i^T}(s\boldsymbol{I} - \boldsymbol{A_i})^{-1}\boldsymbol{b_{pi}} + d_{pi} \\ G_{qi}(s) &= \boldsymbol{c_i^T}(s\boldsymbol{I} - \boldsymbol{A_i})^{-1}\boldsymbol{b_{qi}} + d_{qi} \end{aligned}$.

By combining Eqs 1, 2, there is a clear expression for the SG-*i* model. Therefore, the model of the whole system is derived by combining PMSGs and SGs.

2.2 Voltage oscillation loop of the PMSG

Figure 2 depicts the PMSG-*k* structure coupled to the power system. X_{fk} represents the reactance, C_k refers to the DC capacitor, and V_{dck} is the magnitude of the DC capacitor voltage.

Consider the PCC-*k* ($V_{PCC-k}\angle\theta_{PCC-k}$)'s voltage direction to be the *d*-axis of the PMSG-*k*'s *d*–*q* coordinate. Thus,

$$V_{dk} = V_k,\ V_{qk} = 0, \tag{3}$$

where subscripts *d* and *q* stand for *d*- and *q*-axis components in the *d*–*q* coordinate, respectively.

The model of PMSG-*k* can be determined as follows (Li et al., 2012; Du et al., 2017):

$$\begin{aligned} \frac{d}{dt}\boldsymbol{\Delta X_k} &= \boldsymbol{A_k \Delta X_k} + \boldsymbol{b_k}\Delta V_k \\ \Delta P_k &= \boldsymbol{c_{pk}^T \Delta X_k} + d_{pk}\Delta V_k \\ \Delta Q_k &= \boldsymbol{c_{qk}^T \Delta X_k} + d_{qk}\Delta V_k \end{aligned}, \tag{4}$$

where $\boldsymbol{\Delta X_k}$, (k = 1, 2., N) represents the PMSG-*k* state value matrix.

From Figure 2, the equations of active and reactive power outputs of PMSG-k are obtained as follows:

$$\begin{aligned} \Delta P_k &= V_{k0}\Delta I_{dk} + I_{dk0}\Delta V_k \\ \Delta Q_k &= -V_{k0}\Delta I_{qk} - I_{qk0}\Delta V_k \end{aligned}, \tag{5}$$

where the variable at the steady state is denoted by subscript 0.

In this way, the currents of PMSG-*k* can be obtained as

$$\begin{aligned} X_{fk}\frac{dI_{dk}}{dt} &= \omega_0(V_{sdk} - V_{dk}) + \omega_0 X_{fk} I_{qk} \\ X_{fk}\frac{dI_{qk}}{dt} &= \omega_0\left(V_{sqk} - V_{qk}\right) - \omega_0 X_{fk} I_{dk} \end{aligned}, \tag{6}$$

where ω_0 is the synchronous frequency.

By combining Eqs 3–6, the linearized line current equations could be written as Eq. 7.

$$\begin{aligned} X_{fk}\frac{d\Delta I_{dk}}{dt} &= \omega_0(\Delta V_{sdk} - \Delta V_k) + \omega_0 X_{fk}\Delta I_{qk} \\ X_{fk}\frac{d\Delta I_{qk}}{dt} &= \omega_0\Delta V_{sqk} - \omega_0 X_{fk}\Delta I_{dk} \end{aligned}. \tag{7}$$

Figure 3 shows the configuration of the MSC vector control of PMSG-*k*, and there are three control loops in Figure 3: part 1 is speed

TABLE 4 Computational results of the dynamic index from each of the rest of PMSGs—study case 3.

	$K_{p\text{-}3}$	$K_{i\text{-}3}$	X_{f4}	X_{f5}	H_2	H_3	H_4	H_5
Case 1	0.22	250	0.27	0.305	1.8378	24.3620	0.0029	**−0.0909**
Case 2	0.24	215	0.27	0.18	1.5030	19.8813	0.0024	**−0.0729**
Case 3	0.35	200	0.27	0.18	1.2047	15.8234	0.0019	**−0.0583**
Case 4	0.1	225	0.27	0.305	1.8036	23.9910	0.0028	**−0.0892**
Case 5	0.22	210	0.27	0.18	1.4901	19.7228	0.0023	**−0.0723**
Case 6	0.1	225	0.27	0.18	1.8037	23.9915	0.0028	**−0.0876**
Case 7	1.2	180	0.27	0.18	0.6670	14.4086	**−0.0004**	0.0138
Case 8	1.2	170	0.355	0.18	0.3570	15.5686	**−0.0005**	0.0180
Case 9	1	190	0.27	0.18	0.1256	0.9659	0.0002	**−0.0054**
Case 10	1	230	0.27	0.18	0.4734	5.6057	0.0008	**−0.0223**
Case 11	0.8	200	0.27	0.305	0.5178	6.3402	0.0008	**−0.0255**
Case 12	1.05	200	0.27	0.2	0.1362	1.0722	0.0003	**−0.0060**

The bold values means in this table means the negative index.

control, part 2 is q-axis current control, and part 3 is d-axis current control.

From Figure 3, the model of the three loops of the MSC vector control can be obtained as Eq. 8.

$$\begin{aligned}\Delta I_{pqk}^{ref} &= \Delta\omega_{pk}\left(K_{p-5}+\frac{K_{i-5}}{s}\right)\\ \Delta V_{pqk}^{ref} &= \left(\Delta I_{pqk}-\Delta I_{pqk}^{ref}\right)\left(K_{p-6}+\frac{K_{i-6}}{s}\right)-\psi_f\Delta\omega_{pk}\\ &\quad -X_{pdk}\left(\omega_{pk0}\Delta I_{pdk}+I_{pdk0}\Delta\omega_{pk}\right),\\ \Delta V_{pdk}^{ref} &= \Delta I_{pdk}\left(K_{p-7}+\frac{K_{i-7}}{s}\right)+X_{pqk}\left(\omega_{pk0}\Delta I_{pqk}+I_{pqk0}\Delta\omega_{pk}\right)\end{aligned}\quad (8)$$

where V_{pqk}^{ref} and V_{pdk}^{ref} represent the q- and d-axis components of the reference voltage of MSC, respectively.

Figure 4 shows the configuration of the GSC vector control of PMSG-*k*. There are four control loops in Figure 4: part 1 is DC voltage control, part 2 is d-axis current control, part 3 is reactive power control, and part 4 is q-axis current control.

From Figure 4, the model of four loops can be obtained as Eqs 9–10.

$$\begin{aligned}\Delta I_{dk}^{ref} &= \Delta V_{dck}\left(K_{p-1}+\frac{K_{i-1}}{s}\right)\\ \Delta V_{sdk}^{ref} &= \left(\Delta I_{dk}^{ref}-\Delta I_{dk}\right)\left(K_{p-2}+\frac{K_{i-2}}{s}\right)+\Delta V_{dk}-X_{fk}\Delta I_{qk}\end{aligned},\quad (9)$$

$$\begin{aligned}\Delta I_{qk}^{ref} &= \Delta Q_k\left(K_{p-3}+\frac{K_{i-3}}{s}\right)\\ \Delta V_{sqk}^{ref} &= \left(\Delta I_{qk}^{ref}-\Delta I_{qk}\right)\left(K_{p-4}+\frac{K_{i-4}}{s}\right)+\Delta V_{qk}+X_{fk}\Delta I_{dk}\end{aligned}.\quad (10)$$

By ignoring the transient process of the PWM algorithm, the following equations can be obtained as

$$V_{sdk}^{ref}=V_{sdk},\ V_{sqk}^{ref}=V_{sqk}.\quad (11)$$

By combining Eqs 5, 10, 11, the linearized equation containing ΔV_{sqk}, ΔV_k, ΔI_{dk}, and ΔI_{qk} can be written as Eq. 12.

$$\begin{aligned}&\Delta V_{sqk}+I_{qk0}\left(K_{p-3}+\frac{K_{i-3}}{s}\right)\left(K_{p-4}+\frac{K_{i-4}}{s}\right)\Delta V_k=\\ &X_{fk}\Delta I_{dk}-\left[V_{k0}\left(K_{p-3}+\frac{K_{i-3}}{s}\right)+1\right]\left(K_{p-4}+\frac{K_{i-4}}{s}\right)\Delta I_{qk}\end{aligned}.\quad (12)$$

By substituting Eq. 7 in Eq. 12, the transfer function model from variable ΔV_k to variable ΔI_{qk} is then deduced as Eq. 13.

$$\Delta I_{qk}=G_{IVk}(s)\Delta V_k,\quad (13)$$

where $G_{IVk}(s)=\frac{-\omega_0 I_{qk0}(sK_{p-3}+K_{i-3})(sK_{p-4}+K_{i-4})}{\omega_0[V_{k0}(sK_{p-3}+K_{i-3})+s](sK_{p-4}+K_{i-4})+s^3X_{fk}}$.

By combining Eqs 5, 13, the linearized model of the voltage oscillation loop of PMSG-*k* can be deduced as Eq. 14. In addition, the configuration is shown in Figure 5.

$$\Delta Q_k=-I_{qk0}\Delta V_k-V_{k0}\Delta I_{qk}=-\left[I_{qk0}+V_{k0}G_{IVk}(s)\right]\Delta V_k.\quad (14)$$

Then, the transfer function model from ΔQ_k to ΔV_k of the PMSG-*k* can be written as

$$\Delta V_k=G_{QVk}(s)\Delta Q_k,\quad (15)$$

where $G_{QVk}(s)=\frac{-1}{I_{qk0}+V_{k0}G_{IVk}(s)}$.

2.3 Interconnected model of the power system with multi-PMSGs

The proposed model focuses on the dynamic voltage stability under a small signal; in Section 2.2, the voltage oscillation loop of PMSG is derived by linearizing the dynamic equation at a stable equilibrium point. Furthermore, in order to connect all PMSGs, the Q–V sensitivity matrix under the stable equilibrium point can be used as the feedback of the interconnected system.

A linear expression Eq. 16 can be used to represent the relationship between power and voltage.

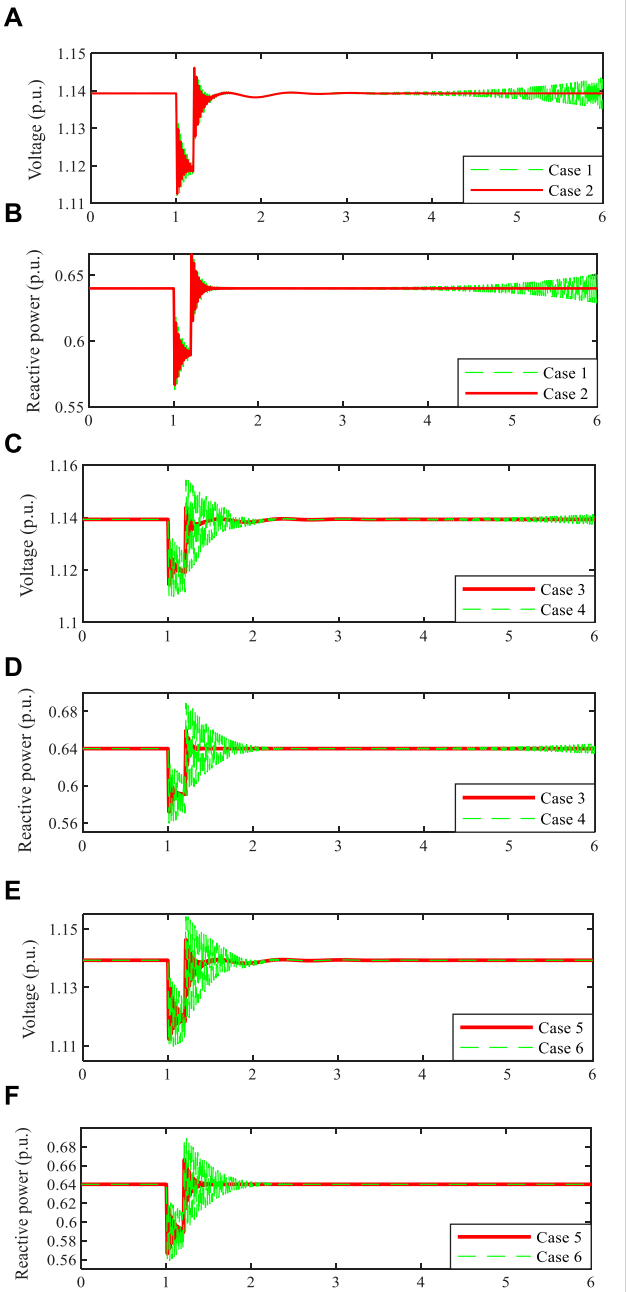

FIGURE 14
(Continued).

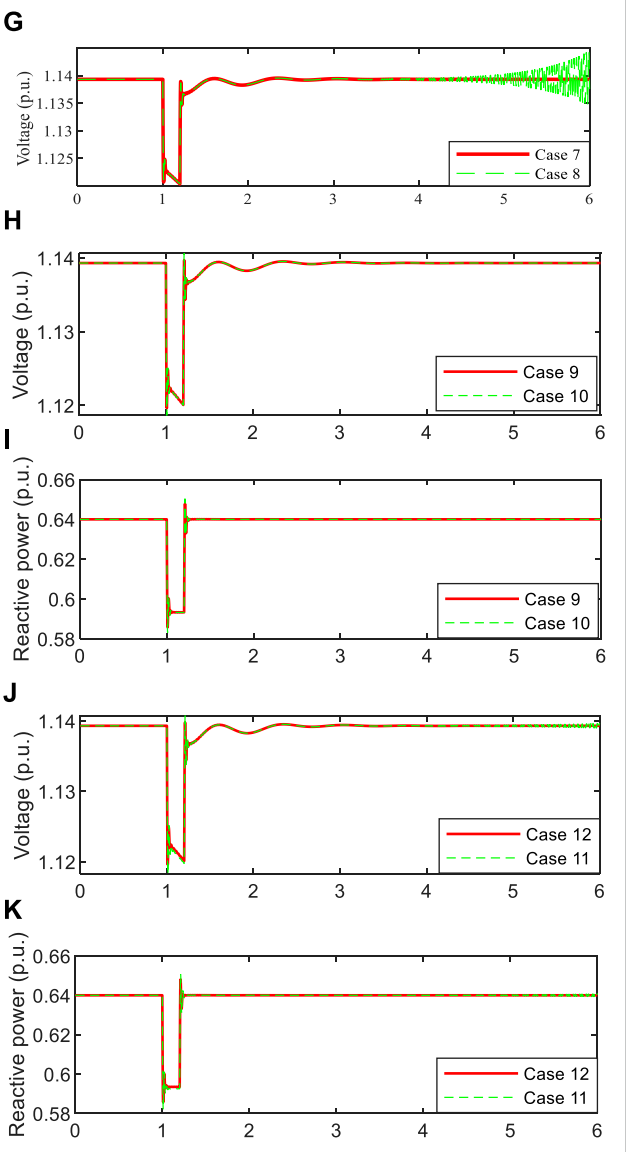

FIGURE 14
(Continued). Dynamic responses of voltage and reactive power of PMSG-1 under different cases.,

$$\begin{bmatrix} \boldsymbol{\Delta P_P} \\ \boldsymbol{\Delta Q_P} \end{bmatrix} = \begin{bmatrix} \boldsymbol{A_{P\theta\_P}} & \boldsymbol{A_{PV\_P}} \\ \boldsymbol{A_{Q\theta\_P}} & \boldsymbol{A_{QV\_P}} \end{bmatrix} \begin{bmatrix} \boldsymbol{\Delta \theta_P} \\ \boldsymbol{\Delta V_P} \end{bmatrix}, \tag{16}$$

where $\boldsymbol{\Delta P_P}$, $\boldsymbol{\Delta Q_P}$, $\boldsymbol{\Delta \theta_P}$, and $\boldsymbol{\Delta V_P}$ are the vectors of the variables of active power, reactive power, angle, and magnitude of voltage, respectively. The subscript P represents the vectors regarding the PCC of PMSGs. $\boldsymbol{\Delta V_P} = [\,\Delta V_1 \;\; \ldots \;\; \Delta V_k \;\; \ldots \;\; \Delta V_N\,]^T$, and V_k is the magnitude of PCC-k voltage in Figure 1.

The voltage stability of the power system is affected by active and reactive power. However, at each operating point, active power could be constant to analyze voltage stability considering the relationship between $\boldsymbol{\Delta Q_P}$ and $\boldsymbol{\Delta V_P}$. Although $\boldsymbol{\Delta P_P}$ is ignored, the influence of the change in system load or power transmission level is included in the relationship between $\boldsymbol{\Delta Q_P}$ and $\boldsymbol{\Delta V_P}$. Based on the above considerations, if $\Delta \boldsymbol{P_P} = \boldsymbol{0}$, then Eq. 17 can be written as

$$\boldsymbol{\Delta Q_P} = \boldsymbol{A_R \Delta V_P}, \tag{17}$$

where $\boldsymbol{A_R} = \boldsymbol{A_{QV\_P}} - \boldsymbol{A_{Q\theta\_P} A_{P\theta\_P}^{-1} A_{PV\_P}}$. $\boldsymbol{A_R}$ is the Q–V sensitivity matrix of the PCC in Figure 1; moreover, it relates to voltage magnitude and reactive power injection.

By combining Eqs 15, 17, the interconnected model of the system integrated with multi-PMSGs can be shown in Figure 6.

There are two parts in Figure 6: part 1 refers to the voltage oscillation loop of PMSG-*k* and part 2 is the whole power system except PMSG-*k*. In Figure 6, part 2 has an influence on the voltage oscillation loop of PMSG-*k*. Moreover, the mathematical expressions

of influence from the network and each PMSG except PMSG-k, respectively, are derived in Section 3. All the PMSGs are connected through the network, and $\boldsymbol{A_R}$ relating to $\Delta\boldsymbol{Q_P}$ and $\Delta\boldsymbol{V_P}$ represents the connection of the network. The mathematical expression of $\Delta\boldsymbol{Q_P}$ in Figure 6 is shown as Eq. 18.

$$\boldsymbol{\Delta Q_P} = \left[\ \Delta Q_1\ \ \ldots\ \ \Delta Q_k\ \ \ldots\ \ \Delta Q_N\ \right]^T. \tag{18}$$

The mathematical expression of $\Delta\boldsymbol{V_P}$ in Figure 6 is shown as Eq. 19.

$$\boldsymbol{\Delta V_P} = \left[\ \Delta V_1\ \ \ldots\ \ \Delta V_k\ \ \ldots\ \ \Delta V_N\ \right]^T. \tag{19}$$

3 Dynamic voltage stability index

From Figures 5, 6, there is a voltage oscillation loop of PMSG-k, which is affected by the rest of the system. To quantify the influence, the dynamic voltage stability index is proposed, and the voltage stability can be analyzed quantitatively. The more detailed derivation can be shown as follows.

For the loop of PMSG-k in Figure 5, Eq. 15 (Sravan Kumar et al., 2014) can be rewritten as

$$\left(s^2 + \mu_k s + K_k\right)\Delta V_k = H_{k1}(s)\Delta Q_k, \tag{20}$$

where, $\mu_k = \frac{\omega_0 K_{p-4}}{X_{fk}}$, $K_k = \frac{\omega_0 K_{i-4}}{X_{fk}}$, and

$$\begin{aligned} H_{k1}(s) = &-\frac{1}{I_{qk0}}s^2 - \frac{\omega_0 K_{p-4} + \omega_0 V_{k0} K_{p-3} K_{p-4}}{I_{qk0} X_{fk}}s \\ &- \frac{\omega_0 K_{i-4} + \omega_0 V_{k0} K_{p-3} K_{i-4} + \omega_0 V_{k0} K_{i-3} K_{p-4}}{I_{qk0} X_{fk}} \\ &- \frac{\omega_0 V_{k0} K_{i-3} K_{i-4}}{I_{qk0} X_{fk}}\frac{1}{s}. \end{aligned}$$

Then, Eq. 17 can be rewritten as

$$\begin{bmatrix} \Delta Q_k \\ \boldsymbol{\Delta Q_S} \end{bmatrix} = \begin{bmatrix} A_{r(k,k)} & \boldsymbol{A_{R(k,S)}} \\ \boldsymbol{A_{R(S,k)}} & \boldsymbol{A_{R(S,S)}} \end{bmatrix} \begin{bmatrix} \Delta V_k \\ \boldsymbol{\Delta V_S} \end{bmatrix}, \tag{21}$$

where subscript k represents the variables of PMSG-k and subscript S represents the variables of all the PMSGs except PMSG-k, $S = 1, 2,., k\text{-}1, k\text{+}1,., N$. Furthermore,

$$\begin{aligned} \boldsymbol{A_{R(k,S)}} &= \left[\ A_{r(k,1)}\ \cdots\ A_{r(k,k-1)}\ A_{r(k,k+1)}\ \cdots\ A_{r(k,N)}\ \right], \\ \boldsymbol{A_{R(S,k)}} &= \left[\ A_{r(1,k)}\ \cdots\ A_{r(k-1,k)}\ A_{r(k+1,k)}\ \cdots\ A_{r(N,k)}\ \right]^T, \\ \boldsymbol{A_{R(S,S)}} &= \begin{bmatrix} A_{r(1,1)} & \cdots & A_{r(1,k-1)} & A_{r(1,k+1)} & \cdots & A_{r(1,N)} \\ \vdots & \ddots & \vdots & \vdots & & \vdots \\ A_{r(k-1,1)} & \cdots & A_{r(k-1,k-1)} & A_{r(k-1,k+1)} & \cdots & A_{r(k-1,N)} \\ A_{r(k+1,1)} & \cdots & A_{r(k+1,k-1)} & A_{r(k+1,k+1)} & \cdots & A_{r(k+1,N)} \\ \vdots & & \vdots & \vdots & \ddots & \vdots \\ A_{r(N,1)} & \cdots & A_{r(N,k-1)} & A_{r(N,k+1)} & \cdots & A_{r(N,N)} \end{bmatrix}. \end{aligned}$$

From Figure 6, the equation $\Delta V_k = G_{QVk}(s)\Delta Q_k$ can be translated into the matrix form as

$$\boldsymbol{\Delta V_S} = \boldsymbol{G_{QVS}(s)\Delta Q_S}, \tag{22}$$

where

$$\boldsymbol{G_{QVS}(s)} = \begin{bmatrix} G_{QV1}(s) & \cdots & \cdots & 0 \\ & \ddots & & \\ \vdots & G_{QVk-1}(s) & & \vdots \\ \vdots & & G_{QVk+1}(s) & \vdots \\ & & & \ddots \\ 0 & \cdots & \cdots & G_{QVN}(s) \end{bmatrix}.$$

By substituting Eqs 21, 22, the transfer function model from variable ΔV_k to variable ΔQ_k is then deduced as Eq. 23.

$$\Delta Q_k = \left[A_{r(k,k)} + \boldsymbol{A_{R(k,S)}G_{QVS}(s)}\left(\boldsymbol{I} - \boldsymbol{A_{R(S,S)}G_{QVS}(s)}\right)^{-1}\boldsymbol{A_{R(S,k)}}\right]\Delta V_k, \tag{23}$$

where $\boldsymbol{I}$ refers to the identity matrix.

Consider $H_{k2}(s)$ as the transfer function of the whole power system except PMSG-k (part 2 in Figure 6). We have

$$\Delta Q_k = H_{k2}(s)\Delta V_k, \tag{24}$$

where

$H_{k2}(s) = A_{r(k,k)} + \boldsymbol{A_{R(k,S)}G_{QVS}(s)}\left(\boldsymbol{I} - \boldsymbol{A_{R(S,S)}G_{QVS}(s)}\right)^{-1}\boldsymbol{A_{R(S,k)}}$.

By substituting Eqs 20, 24, the representative equation of the voltage oscillation loop of PMSG-k is obtained.

$$s^2 + \mu_k s + K_k + H_k(s) = 0, \tag{25}$$

where $H_k(s) = -H_{k1}(s)H_{k2}(s)$.

Consider $\lambda_k = \xi_k + j\omega_k$ as the oscillation mode, which is exactly the mode of the voltage oscillation loop of PMSG-k. Moreover, $\lambda_k = \xi_k + j\omega_k$ is a solution to Eq. 25. Therefore, we obtain

$$\lambda_k^2 + \mu_k\lambda_k + K_k + H_k(\lambda_k) = 0. \tag{26}$$

The decomposition of $H_k(\lambda_k)$ can be obtained as

$$\begin{aligned} H_k(\lambda_k) &= H_{k-real}(\lambda_k) + jH_{k-imag}(\lambda_k) = H_{ks} + H_{kd}\lambda_k \\ &= H_{ks} + H_{kd}(\xi_k + j\omega_k), \end{aligned} \tag{27}$$

where $H_{k-real}(\lambda_k)$ and $H_{k-imag}(\lambda_k)$ are the real and imaginary parts of $H_k(\lambda_k)$, respectively. H_{ks} and H_{kd} are two real numbers, which are presented for the division of $H_k(\lambda_k)$, as denoted in Eq. 27.

Using Eq. 27, H_{ks} and H_{kd} can be calculated as

$$H_{ks} = H_{k-real}(\lambda_k) - \frac{H_{k-imag}(\lambda_k)\xi_k}{\omega_k},\ H_{kd} = \frac{H_{k-imag}(\lambda_k)}{\omega_k}. \tag{28}$$

By substituting Eqs 26, 27, we have

$$\lambda_k^2 + (\mu_k + H_{kd})\lambda_k + K_k + H_{ks} = 0. \tag{29}$$

In Eq. 29, $\mu_k + H_{kd}$ is referred to as the influence on the voltage oscillation loop, where μ_k refers to the self-influence that PMSG-k itself has and H_{kd} is the influence from the power system except PMSG-k. Furthermore, the influence $\mu_k + H_{kd}$ is the component in the variation of voltage $s\Delta V_k$, which is at the complex frequency $\lambda_k = \xi_k + j\omega_k$. Therefore, the speed of voltage variation at the complex frequency represents the physical meaning of influence. The damping ratio and frequency of the oscillation mode λ_k are determined by $\mu_k + H_{kd}$ and $K_k + H_{ks}$, respectively.

In order to calculate the influence from network and each PMSG except PMSG-k, respectively, the derivation is shown as follows.

By combining Eq 23, 24, we obtain Eqs 30, 31.

$$\begin{aligned}\boldsymbol{F}(\boldsymbol{s}) &= \boldsymbol{A}_{\boldsymbol{R}(\boldsymbol{k},\boldsymbol{S})}\boldsymbol{G}_{\boldsymbol{QVS}}(\boldsymbol{s})\left(\boldsymbol{I}-\boldsymbol{A}_{\boldsymbol{R}(\boldsymbol{S},\boldsymbol{S})}\boldsymbol{G}_{\boldsymbol{QVS}}(\boldsymbol{s})\right)^{-1}\\ &= \left[\, f_1(s) \;\cdots\; f_{k-1}(s) \;\; f_{k+1}(s) \;\cdots\; f_N(s) \,\right].\end{aligned} \tag{30}$$

Hence,

$$H_{k2}(s) = A_{r(k,k)} + \sum_{\substack{i=1\\ i\neq k}}^{N} f_i(s)A_{r(i,k)}, \tag{31}$$

where $f_i(s)A_{r(i,k)}$ refers to the effect coefficient of PMSG-i and $A_{r(k,k)}$ is the effect coefficient of the network.

Thus, the dynamic voltage stability index, i.e., the influence from network and each PMSG except PMSG-k, respectively, can be obtained as Eqs 32–33.

$$H_{kd-net} = \frac{1}{\omega_k}\mathrm{Im}\left[-A_{r(k,k)}H_{k1}(\lambda_k)\right], \tag{32}$$

$$H_{kd-PMSG-i} = \frac{1}{\omega_k}\mathrm{Im}\left[-f_i(\lambda_k)A_{r(i,k)}H_{k1}(\lambda_k)\right], \tag{33}$$

where H_{kd-net} refers to the influence from the network on the voltage oscillation loop of PMSG-k and $H_{kd-PMSG-i}$ is the influence from PMSG-i. The symbol Im [ ] means the imaginary part of the variable.

4 Example of the test system

The formation of the example of the test system with PMSGs is illustrated in Figure 7. There are four SGs and five PMSGs in the power system. The model of the PMSG provided by Li et al. (2012) is adopted, and the values of the parameters of PMSGs are adjusted differently according to the parameters of SGs and loads.

4.1 Study case 1—calculation of the dynamic voltage stability index

In this study case, the oscillation loop of the PMSG-1 is chosen for the calculation of the dynamic index of the rest of the PMSGs. The equation of the chosen voltage oscillation loop of the PMSG-1 is obtained from Eq. 25.

$$s^2 + D_1 s + K_1 = s^2 + 173.33s + 1841.6 = 0. \tag{34}$$

Thus, the following estimation of voltage oscillation mode λ_1 can be obtained by solving Eq. 34. The frequency of the voltage oscillation is 16.62 Hz.

$$\lambda_1 = -86.67 - j104.43\,(rad./s.).$$

By combining the estimation of the oscillation mode and Eq. 33, the dynamic index from each of the rest of the PMSGs to the chosen voltage oscillation loop could be calculated, and the computational results are shown in Table 1. From Table 1, it is evident that PMSG-2, PMSG-3, and PMSG-4 provide the positive index, and PMSG-3 provides the maximum positive index, but PMSG-5 provides the negative index.

To validate the effectiveness of the calculation of the dynamic index, each of the rest of the PMSGs is shed subsequently. The results of the non-linear simulation carried out are shown in Figures 8, 9. At t = 1s, the reactive power of PMSG-1 decreases by 0.1 p.u. for 0.2 s. Figures 8, 9 show dynamic responses of reactive power and voltage of PMSG-1 with different PMSGs shed, respectively. The system tends to be unstable after a small disturbance without PMSGs shed. From the calculated voltage stability index in Table 1, the index related to PMSG-5 is negative, which implies the troublemaker of the oscillation. Hence, the dynamic index of different PMSGs can be calculated, and the source of voltage oscillation can be identified using the dynamic index.

4.2 Study case 2—impact of reactance of the filtering reactor

PMSG-k is connected to the power system via the transmission line, which is represented by the filtering reactor X_{fk}. In study case 1, X_{f5} is 0.32. In order to evaluate the impact of the reactance of the filtering reactor on the dynamic index, X_{f5} is changed from 0.32 to 0.18 in study case 2. Figure 10 shows the variation curve of the dynamic index of PMSG-5. It can be seen that decreasing X_{f5} can reduce the amplitude of the negative index supplied by PMSG-5.

Then, the computational results of the dynamic index are shown in Table 2 after X_{f5} is changed to 0.18. Comparing Tables 1, 2, the dynamic index from PMSG-2, PMSG-3, and PMSG-4 is almost constant, but the negative index supplied by PMSG-5 is reduced.

In order to study the impact of the decreasing negative index, which is caused by the decreasing reactance to the voltage oscillation loop of PMSG-1, a non-linear simulation is carried out, and the dynamic responses of reactive power and voltage of PMSG-1 under different conditions of filtering reactors are shown in Figure 11.

Furthermore, the control parameters of PMSG have been appropriately adjusted, $K_{p\text{-}3}$ is changed to 1 and $K_{i\text{-}3}$ is changed to 200. Then, the computational results of the dynamic index are shown in Table 3; it can also be seen that the negative index supplied by PMSG-5 is decreased when X_{f5} is changed from 0.305 to 0.18. The results of the non-linear simulation carried out are shown in Figure 12; at t = 1s, the reactive power of PMSG-1 decreases by 0.1 p.u. for 0.2 s. The system tends to be more stable after a small disturbance when X_{f5} is 0.18.

It is evident that decreasing the reactance of the line that connects the source of oscillation to the external grid could reduce the risk of voltage oscillations. The results in Figures 10–12 confirm the correctness of the calculation of the dynamic index.

4.3 Study case 3—impact of parameters of the GSC vector control

From the derivation of the voltage oscillation loop shown in Section 2, the parameters $K_{p\text{-}3}$ and $K_{i\text{-}3}$ (parameters of part 3 in Figure 4) of the selected PMSG may have an influence on the voltage

oscillation loop of the selected PMSGs. The parameters of PMSG-1 in case study 1 are as follows: $K_{p\text{-}3}$ = 0.1 and $Ki\text{-}3$ = 250.

To examine the influence of the parameters $K_{p\text{-}3}$ and $K_{i\text{-}3}$ on the dynamic index, $K_{p\text{-}3}$ is changed from 0.1 to 0.35 and $K_{i\text{-}3}$ is changed from 250 to 200 in case study 3. Figure 13 shows the variation curve of the dynamic index of PMSG-5 when the parameters are changing. There are 12 variation curves in Figure 13, the first six curves represent the variation of the dynamic index of PMSG-5 when $K_{p\text{-}3}$ is constant and $K_{i\text{-}3}$ is decreasing, while the last six curves represent the variation of the dynamic index when $K_{i\text{-}3}$ is constant and $K_{p\text{-}3}$ is increasing under different conditions of X_{f5}. From Figure 13, it can be seen that the risk of voltage oscillations can be reduced by decreasing $K_{i\text{-}3}$ and increasing $K_{p\text{-}3}$. Furthermore, adjusting the parameter $K_{p\text{-}3}$ and $K_{i\text{-}3}$ could be more flexible and effective at reducing the negative dynamic index rather than decreasing X_{f5}.

Table 4 shows the computational results of the dynamic index in eight cases with different conditions of $K_{p\text{-}3}$, $K_{i\text{-}3}$, X_{f4}, and X_{f5}, where H_2, H_3, H_4, and H_5 refer to the dynamic index of PMSG-2–PMSG-5, respectively. From Table 3, only PMSG-5 provides the negative index in cases 1–6 and cases 9–12, and the negative index is supplied by PMSG-4 in cases 7 and 8.

To validate the correctness of the calculation of the dynamic index, a non-linear simulation is carried out. Figures 14A–K shows the dynamic responses of PMSG-1 under different cases presented by Table 4, including the dynamic responses of reactive power and voltage. The risk of oscillation increases when the negative index supplied by the source of oscillation (i.e., PMSG-5) increases in cases 1–6 and cases 9–12. Moreover, the source of oscillation is PMSG-4 in cases 7 and 8, and the system tends to be unstable, obviously after disturbance in case 8, which has a larger negative index. Hence, the correctness of the calculation is verified, and the dynamic voltage stability index can be applied under different conditions.

5 Conclusion

This paper presents a dynamic voltage stability index based on the voltage oscillation loop for a power system with multi-PMSGs, and the correctness of the index is confirmed by the test system. The primary contributions are listed as follows:

(1) The voltage oscillation loop existing in the PMSGs is derived through merging the dynamic model of PMSGs. Furthermore, the Q–V sensitivity matrix is used as feedback to connect all the PMSGs, and then the model applied to study voltage stability is obtained.
(2) The dynamic interaction on voltage stability for the power system integrated with multi-PMSGs could be quantified by applying the dynamic index proposed in this paper. The influence of the rest of each PMSG on the voltage oscillation loop of the selected PMSG could be calculated, and the source of voltage oscillation that provides the maximum negative index could be identified.
(3) The proposed dynamic voltage stability index is able to be applied to direct the control parameters adjustment of selected PMSG to ensure that voltage stability is maintained under different conditions.

The main drawback of this strategy is that it is based on the model of wind power grid-connected systems to quantitatively analyze the dynamic voltage stability among PMSGs. This method is more suitable for offline analysis of the system and makes it difficult to conduct real-time online quantitative analysis of the voltage characteristics of wind power grid-connected systems. Therefore, the authors will conduct research on online quantitative analysis of the dynamic voltage stability of the wind power grid-connected system based on measurement data in the next step.

Data availability statement

The original contributions presented in the study are included in the article/Supplementary material; further inquiries can be directed to the corresponding author.

Author contributions

LC: methodology and writing–original draft. JW: writing–review and editing. XK: writing–review and editing. ZH: writing–review and editing. DA: writing–review and editing.

Funding

The author(s) declare that no financial support was received for the research, authorship, and/or publication of this article.

Conflict of interest

Authors JW and XK were employed by the Northwest Branch of State Grid Corporation of China.

The remaining authors declare that the research was conducted in the absence of any commercial or financial relationships that could be construed as a potential conflict of interest.

Publisher's note

References

Adams, J., Pappu, V. A., and Dixit, A. (2012). "*Ercot experience screening for Sub-Synchronous Control Interaction in the vicinity of series capacitor banks*," IEEE Power and Energy Society General Meeting, San Diego, CA, pp. 1–5.

Baa Wafaa, M., and Dessaint, L. (2018). Approach to dynamic voltage stability analysis for DFIG wind parks integration. *IET Renew. Power Gener.* 12 (2), 190–197. doi:10.1049/iet-rpg.2016.0482

Belkhier, Y., and Oubelaid, A. (2024). Novel design and adaptive coordinated energy management of hybrid fuel-cells/tidal/wind/PV array energy systems with battery storage for microgrids. *Energy Storage* 6, e556. doi:10.1002/est2.556

Chi, Y., and Xu, Y. (2020). Multi-stage coordinated dynamic VAR source placement for voltage stability enhancement of wind-energy power system. *IET Generation, Transm. Distribution* 14 (6), 1104–1113. doi:10.1049/iet-gtd.2019.0126

Dashtdar, M., et al. (2022). "Protection of DC microgrids based on frequency domain analysis using fourier transform," *IEEE 3rd KhPI week on advanced Technology (KhPIWeek)*, Kharkiv, Ukraine, pp. 1–6.

Du, W., Bi, J., Cao, J., and Wang, H. F. (2016). A method to examine the impact of grid connection of the DFIGs on power system electromechanical oscillation modes. *IEEE Trans. Power Syst.* 31 (5), 3775–3784. doi:10.1109/tpwrs.2015.2494082

Du, W., Chen, X., and Wang, H. F. (2017). Power system electromechanical oscillation modes as affected by dynamic interactions from grid-connected PMSGs for wind power generation. *IEEE Trans. Sustain. Energy* 8 (3), 1301–1312. doi:10.1109/tste.2017.2677094

Erlich, I. (2017). "Control challenges in power systems dominated by converter interfaced generation and transmission technologies," NEIS 2017; Conference on Sustainable Energy Supply and Energy Storage Systems, 21-22 September 2017, Hamburg, Germany, IEEE, 1–8.

García, H., Segundo, J., Rodríguez-Hernández, O., Campos-Amezcua, R., and Jaramillo, O. (2018). Harmonic modelling of the wind turbine induction generator for dynamic analysis of power quality. *Energies* 11 (1), 104. doi:10.3390/en11010104

Khosravi, N., Baghbanzadeh, R., Oubelaid, A., Tostado-Véliz, M., Bajaj, M., Hekss, Z., et al. (2023). A novel control approach to improve the stability of hybrid AC/DC microgrids. *Appl. Energy* 344, 121261. doi:10.1016/j.apenergy.2023.121261

Kroposki, B., Johnson, B., Zhang, Y., Gevorgian, V., Denholm, P., Hodge, B. M., et al. (2017). Achieving a 100% renewable grid: operating electric power systems with extremely high levels of variable renewable energy. *IEEE Power Energy Mag.* 15 (2), 61–73. doi:10.1109/mpe.2016.2637122

Li, S., Haskew, T. A., Swatloski, R. P., and Gathings, W. (2012). Optimal and direct-current vector control of direct-driven PMSG wind turbines. *IEEE Trans. Power Electron.* 27 (5), 2325–2337. doi:10.1109/tpel.2011.2174254

Liu, H., and Sun, J. (2014). Voltage stability and control of offshore wind farms with AC collection and HVDC transmission. *IEEE J. Emerg. Sel. Top. Power Electron.* 2 (4), 1181–1189. doi:10.1109/jestpe.2014.2361290

Liu, H., Xie, X., He, J., Xu, T., Yu, Z., Wang, C., et al. (2017). Subsynchronous interaction between direct-drive PMSG based wind farms and weak AC networks. *IEEE Trans. Power Syst.* 32 (6), 4708–4720. doi:10.1109/tpwrs.2017.2682197

Liu, J., Xu, Y., Dong, Z. Y., and Wong, K. P. (2018). Retirement-driven dynamic VAR planning for voltage stability enhancement of power systems with high-level wind power. *IEEE Trans. Power Syst.* 33 (2), 2282–2291. doi:10.1109/tpwrs.2017.2732441

Ou, R., Xiao, X., Zou, Z., Zhang, Y., and Wang, Y. (2016). Cooperative control of SFCL and reactive power for improving the transient voltage stability of grid-connected wind farm with DFIGs. *IEEE Trans. Appl. Supercond.* 26 (7), 1–6. doi:10.1109/tasc.2016.2574344

Qian, Y., Yuan, X., and Zhao, M. (2016). Analysis of voltage control interactions and dynamic voltage stability in multiple wind farms. *2016 IEEE Power Energy Soc. General Meet.*, 1–5. doi:10.1109/PESGM.2016.7741676

Rakhshani, E., Gusain, D., Sewdien, V., Rueda Torres, J. L., and Van Der Meijden, M. A. M. M. (2019). A key performance indicator to assess the frequency stability of wind generation dominated power system. *IEEE Access* 7, 130957–130969. doi:10.1109/access.2019.2940648

Rawat, M. S., and Vadhera, S. (2020). Probabilistic steady state voltage stability assessment method for correlated wind energy and solar photovoltaic integrated power systems. *Energy Technol.* 9 (2), 2000732. doi:10.1002/ente.202000732

Sanchez, A. G., Molina, M. G., and Rizzato Lede, A. M. (2012). Dynamic model of wind energy conversion systems with PMSG-based variable-speed wind turbines for power system studies. *Int. J. hydrogen energy* 37 (13), 10064–10069. doi:10.1016/j.ijhydene.2011.12.077

Sravan Kumar, V. S., Krishna Reddy, K., and Thukaram, D. (2014). Coordination of reactive power in grid-connected wind farms for voltage stability enhancement. *IEEE Trans. Power Syst.* 29 (5), 2381–2390. doi:10.1109/tpwrs.2014.2300157

Su, G., Xu, L., Du, W., Chen, C., Ji, Y., and Wang, H. (2019). Power system dynamic voltage stability affected by open-loop modal coupling between DFIG-based wind farms and IM loads. *J. Eng.* 2019 (16), 2514–2519. doi:10.1049/joe.2018.8579

Tourandaz Kenari, M., Sepasian, M. S., and Setayesh Nazar, M. (2019). Probabilistic assessment of static voltage stability in distribution systems considering wind generation using catastrophe theory. *IET Generation, Transm. Distribution* 13 (13), 2856–2865. doi:10.1049/iet-gtd.2018.5497

Venkatesh, B., Rost, A., and Chang, L. (2007). Dynamic voltage collapse index— wind generator application. *IEEE Trans. Power Deliv.* 22 (1), 90–94. doi:10.1109/tpwrd.2006.887097

Vittal, E., O'Malley, M., and Keane, A. (2010). A steady-state voltage stability analysis of power systems with high penetrations of wind. *IEEE Trans. Power Syst.* 25 (1), 433–442. doi:10.1109/tpwrs.2009.2031491

Wang, L., Xie, X., Jiang, Q., Liu, H., Li, Y., and Liu, H. (2015b). Investigation of SSR in practical DFIG-based wind farms connected to a series-compensated power system. *IEEE Trans. Power Syst.* 30 (5), 2772–2779. doi:10.1109/tpwrs.2014.2365197

Wang, X., Wei, X., and Meng, Y. (2015a). Experiment on grid-connection process of wind turbines in fractional frequency wind power system. *IEEE Trans. Energy Convers.* 30 (1), 22–31. doi:10.1109/tec.2014.2358498

Wijnhoven, T., Deconinck, G., Neumann, T., and Erlich, I. (2014). "Control aspects of the dynamic negative sequence current injection of type 4 wind turbines," in 2014 IEEE PES General Meeting | Conference and Exposition, MD, USA, 27-31 July 2014 (National Harbor), 1–5.